07 Jun 2018

Evolution of Structure and Superconductivity in $Ba(Ni_{1-x}Co_x)_2As_2$

Chris Eckberg

Limin Wang

Halyna Hodovanets
Missouri University of Science and Technology, halyna.hodovanets@mst.edu

Hyunsoo Kim
Missouri University of Science and Technology, hyunsoo.kim@mst.edu

et. al. For a complete list of authors, see https://scholarsmine.mst.edu/phys_facwork/2177

Recommended Citation

C. Eckberg et al., "Evolution of Structure and Superconductivity in $Ba(Ni_{1-x}Co_x)_2As_2$," *Physical Review B*, vol. 97, no. 22, article no. 224505, American Physical Society (APS), Jun 2018.
The definitive version is available at https://doi.org/10.1103/PhysRevB.97.224505

Evolution of structure and superconductivity in $Ba(Ni_{1-x}Co_x)_2As_2$

Chris Eckberg,[1,*] Limin Wang,[1] Halyna Hodovanets,[1] Hyunsoo Kim,[1] Daniel J. Campbell,[1] Peter Zavalij,[2] Philip Piccoli,[3] and Johnpierre Paglione[1,†]

[1]*Center for Nanophysics and Advanced Materials, Department of Physics, University of Maryland, College Park, Maryland 20742, USA*
[2]*Department of Chemistry, University of Maryland, College Park, Maryland 20742, USA*
[3]*Department of Geology, University of Maryland, College Park, Maryland 20742, USA*

(Received 1 March 2018; revised manuscript received 25 April 2018; published 7 June 2018)

The effects of Co substitution on $Ba(Ni_{1-x}Co_x)_2As_2$ ($0 \leqslant x \leqslant 0.251$) single crystals grown out of Pb flux are investigated via transport, magnetic, and thermodynamic measurements. $BaNi_2As_2$ exhibits a first-order tetragonal to triclinic structural phase transition at $T_s = 137$ K upon cooling, and enters a superconducting phase below $T_c = 0.7$ K. The structural phase transition is sensitive to cobalt content and is suppressed completely by $x \geqslant 0.133$. The superconducting critical temperature, T_c, increases continuously with x, reaching a maximum of $T_c = 2.3$ K at $x = 0.083$ and then decreases monotonically until superconductivity is no longer observable well into the tetragonal phase. In contrast to similar $BaNi_2As_2$ substitutional studies, which show an abrupt change in T_c at the triclinic-tetragonal boundary that extends far into the tetragonal phase, $Ba(Ni_{1-x}Co_x)_2As_2$ exhibits a domelike phase diagram centered around the zero-temperature tetragonal-triclinic boundary. Together with an anomalously large heat capacity jump $\Delta C_e/\gamma T \sim 2.2$ near optimal doping, the smooth evolution of T_c in the $Ba(Ni_{1-x}Co_x)_2As_2$ system suggests a mechanism for pairing enhancement other than phonon softening.

DOI: 10.1103/PhysRevB.97.224505

I. INTRODUCTION

High-temperature superconductivity in Fe-based compounds has taken on immense research interest since their discovery in 2008 [1–4]. Of these compounds, $BaFe_2As_2$ has been among the most extensively studied, largely due to the availability of sizable high-quality single crystals. $BaFe_2As_2$ is an antiferromagnet (AFM) with $T_N = 135$ K [5]. AFM order is closely linked to both electronic nematicity [6] and structural symmetry breaking from tetragonal to orthorhombic [5]. Magnetic and structural transitions present in pure $BaFe_2As_2$ are sensitive to chemical substitution and physical pressure, and a domelike superconducting phase emerges with their suppression [7]. While substitution on all three ionic sites has been observed to stabilize high-T_c superconductivity, the choice of substituent site strongly influences the ensuing superconducting phase. For instance, electron doping with Ni and Co substitution for Fe induces fully gapped superconductivity while isoelectronic substitution of P on the As site produces a nodal superconducting phase [8–11]. Superconductivity in all of these series, however, is believed to be closely linked to phase criticality; specifically, the competition and cooperation between nematic and magnetic phases and superconducting pairing.

$BaNi_2As_2$ crystallizes in the same tetragonal $ThCr_2Si_2$ structure (space group $I4/mmm$) as $BaFe_2As_2$ and similarly undergoes a structural distortion at approximately 135 K [12]. However, in $BaNi_2As_2$ the structural distortion is between a high-temperature tetragonal and low-temperature triclinic, rather than orthorhombic, symmetry, and has no associated magnetic order [13,14]. Rather, theoretical work has suggested that the zigzag chain structure in the triclinic distortion is driven by orbital ordering, explaining the lack of magnetic order [15].

$BaNi_2As_2$ also displays bulk superconductivity below $T_c = 0.7$ K [12], suggested to be conventional BCS type in nature with a fully gapped s-wave order parameter symmetry [16,17]. Superconductivity in $BaNi_2As_2$ is widely thought to be distinct from the unconventional sign-changing, $s^{\pm}$, order parameter of the iron-based high-T_c superconductors [2,18], such as in $Ba(Fe_{1-x}Ni_x)_2As_2$ $0.02 \leqslant x \leqslant 0.08$ [19]. Electronic structure calculations suggest $BaNi_2As_2$ should not host an $s^{\pm}$ state, as any nodal planes would necessarily intersect the Fermi surface due to its complexity [20], and the heat capacity and thermal conductivity data of $BaNi_2As_2$ has been well fit to a BCS s-wave model [16]. Despite the distinctions from its iron-based counterpart, previous substitutional studies in $Ba(Ni_{1-x}Cu_x)_2As_2$ [21] and $BaNi_2(As_{1-x}P_x)_2$ [22] have found an abrupt, strong enhancement of T_c from 0.7 K to 3.3 K upon suppression of the triclinic phase [21,22], with strengthened pairing attributed to a soft phonon mode at the first-order structural phase boundary. The enhanced T_c value in the tetragonal phase of $BaNi_2(As_{1-x}P_x)_2$ extends to the $x = 1$ end member $BaNi_2P_2$ [23], suggesting the enhancement is rooted in the tetragonal structure itself.

The recent discovery of a charge density wave (CDW) emerging near the structural transition in $BaNi_2As_2$ [24] raises new questions about pairing in this system, in particular the possibility of a more complicated relationship between superconductivity and structure in $BaNi_2As_2$. Here we report the physical properties of Co-substituted $BaNi_2As_2$ single crystals, showing that the low-temperature triclinic phase is smoothly suppressed with cobalt substitution concomitant

*eckbergc@umd.edu
†paglione@umd.edu

with a continuous enhancement of T_c upon approach to the zero-temperature structural phase boundary. We find that, in contrast to other reported $BaNi_2As_2$ substitutional studies, and in a manner reminiscent of similar work in $BaFe_2As_2$, $Ba(Ni_{1-x}Co_x)_2As_2$ exhibits a strong enhancement of T_c in both the triclinic and tetragonal low-temperature phases, decreasing away from the zero-temperature suppression of the triclinic phase suggesting a Cooper pairing enhancement reminiscent of superconductivity emerging from quantum criticality.

II. EXPERIMENTAL METHODS

$Ba(Ni_{1-x}Co_x)_2As_2$ crystals were grown out of Pb flux using a solution growth technique originally reported by Ronning *et al.* [12]. Crystals formed as shiny, thin platelets, with typical dimensions of 0.5 mm × 0.5 mm × 0.05 mm with a high observed residual resistivity ratio RRR = 10 that exceeded previous reports, as well as our own self-flux grown samples. The typically small crystal sizes were prohibitive for thermodynamic and magnetic measurements. To circumvent this issue, larger, unsubstituted $BaNi_2As_2$ crystals with dimensions of 2 mm × 2 mm × 0.5 mm were also synthesized out of NiAs self-flux [13] and were used for characterization of the structural transition. All data presented were taken on Pb-grown crystals unless specified otherwise.

Elemental composition in substituted samples was determined using wavelength dispersive spectroscopy (WDS). Crystal properties within a growth show minimal variation, while WDS gives variability in $Ba(Ni_{1-x}Co_x)_2As_2$ Co concentrations of $\Delta x \leqslant 0.01$ for crystals pulled from the same growth. Variation between the nominal x concentration versus the one obtained from WDS is shown in Fig. 1(a).

Structural data were collected on single crystals in a Bruker APEX-II CCD system equipped with a graphite monochromator and a Mo $K\alpha$ sealed tube ($\lambda = 0.71073$ Å), and were refined using the Bruker SHELXTL software package. Crystallographic information collected in the tetragonal phase (250 K) are included in Table I for several representative x values. Atomic positions evolve monotonically across the phase diagram, while low conventional residual values (R_1) confirm high crystal quality. A continuous decrease in a and increase in c lattice parameters with increasing Co concentration is observed across all measured samples, as shown in Fig. 1(b).

Standard density functional theory calculations for pure $BaNi_2As_2$ were conducted using the WIEN2K [25] implementation of the full potential linearized augmented plane wave method in the local density approximation. The k-point mesh was taken to be 11 × 11 × 11, with lattice constants taken from our experimental measurements. Supercell calculations were implemented for Co-substituted cases (i.e., $Ba_4Ni_7CoAs_8$ for $x = 0.125$ and $Ba_2Ni_3CoAs_4$ for $x = 0.250$), and resultant electronic structures unfolded via recently developed first-principles unfolding methods [26].

Transport, heat capacity, and ac magnetic susceptibility data were taken using a Quantum Design Physical Property Measurement System (PPMS-14T) and DynaCool (DC-14T) systems. An environment between 1.8 and 300 K was used in each system. Heat capacity and transport measurements were extended down to 400 mK using a Quantum Design helium-3 refrigerator option compatible with the PPMS. In-plane

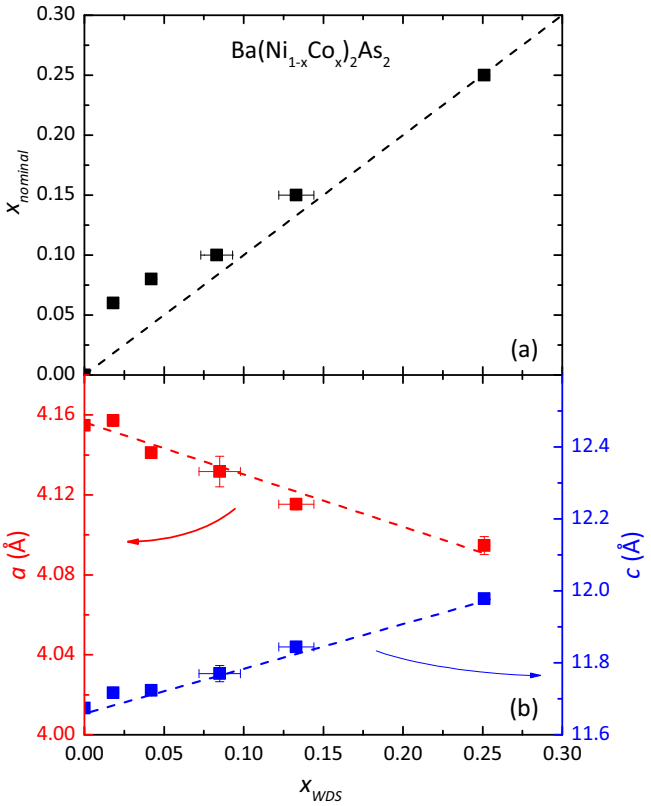

FIG. 1. Structural and chemical characterization of $Ba(Ni_{1-x}Co_x)_2As_2$ single crystals grown from Pb flux. (a) WDS chemical composition characterization for $Ba(Ni_{1-x}Co_x)_2As_2$ single crystals. $x_{WDS} = x_{nominal}$ curve represented by a black dashed line. (b) Lattice parameters in $Ba(Ni_{1-x}Co_x)_2As_2$ series collected at 250 K. Data show a strongly linear evolution in both a- and c-axis length through $x = 0.251$. In some instances error bars are obscured by data points, but are included for all data.

transport data were taken using a four-wire configuration. Au wires were attached to cleaved, or polished when necessary (to remove Pb contamination) single crystals using DuPont 4929N silver paste. Single-crystal ac magnetic susceptibility was measured using a homemade coil [27]. ac magnetic susceptibility measurements between 0.1 and 3 K were taken with the coil mounted on a Quantum Design adiabatic demagnetization refrigerator insert for the PPMS. Data were taken at a frequency of 19.997 kHz, in an ac field with approximate amplitude of 0.25 Oe.

Heat capacity measurements were taken with a relaxation technique fit to a dual time constant model. The background heat capacity of the platform and grease was measured first and subtracted from the final result. Experiments on Co-substituted samples were complicated by small crystal sizes (< 0.1 mg). To circumvent this issue, heat capacity measurements were taken on collections of several samples pulled from the same growth. Sharp anomalies at the structural transitions in measurements taken on these collections of crystals, along with the high degree of growth homogeneity determined through WDS, suggest minimal error in heat capacity data due to collection averaging. The heat capacity data across the first-order structural transition of $BaNi_2As_2$ was measured by establishing ΔT

TABLE I. $Ba(Ni_{1-x}Co_x)_2As_2$ crystallographic data determined through single-crystal x-ray diffraction on crystals grown from Pb flux. All data were collected at 250 K.

x	0	0.083	0.133
Crystal system	Tetragonal	Tetragonal	Tetragonal
Space group	$I4/mmm$	$I4/mmm$	$I4/mmm$
a (Å)	4.144(2)	4.1256(5)	4.1140(7)
b (Å)	4.144(2)	4.1256(5)	4.1140(7)
c (Å)	11.656(6)	11.7486(15)	11.827(2)
V^3 (Å^3)	200.2(2)	199.97(5)	200.17(8)
Reflections	1737	1705	1776
R_1	0.0140	0.0179	0.0156
Atomic parameters:			
Ba	2*a* (0,0,0)	2*a* (0,0,0)	2*a* (0,0,0)
Ni/Co	4*d* (0,1/2,1/4)	4*d* (0,1/2,1/4)	4*d* (0,1/2,1/4)
As	4*e* (0,0,*z*)	4*e* (0,0,*z*)	4*e* (0,0,*z*)
z	0.34726(6)	0.34785(7)	0.34812(6)
Bond lengths (Å):			
Ba-As (Å)	3.4288(15)	3.4213(6)	3.4189(6)
Ni/Co-As (Å)	2.3619(11)	2.3615(5)	2.3618(5)
As-As (Å)	3.560(71)	3.575(0)	3.592(5)
Bond angles (deg):			
As-Ni/Co-As	103.32(2)	103.710(16)	103.971(15)
As-Ni/Co-As	122.63(5)	121.74(4)	121.14(3)

of 15 K at 130 K [28]. Data were collected over 4τ measuring time (about 2.5 min). A single slope method [29] was used to calculate the heat capacity that is shown in the inset (a) to Fig. 2.

dc magnetic susceptibility measurements were carried out in a Quantum Design Magnetic Property Measurement System superconducting quantum interference device magnetometer.

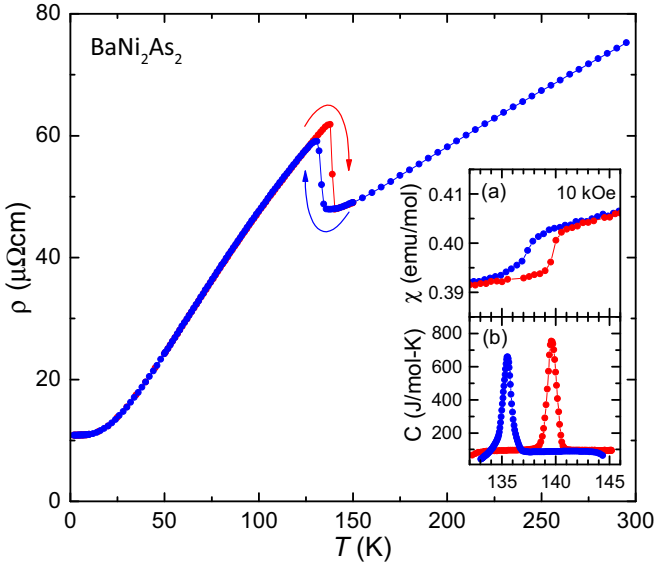

FIG. 2. Characterization of the structural transition in $BaNi_2As_2$ single crystals grown using a self-flux method. Resistivity of $BaNi_2As_2$ single crystal shown in the main figure. Inset (a) [(b)] displays hysteretic magnetization (heat capacity) when warming (red) and cooling (blue) through the structural transition.

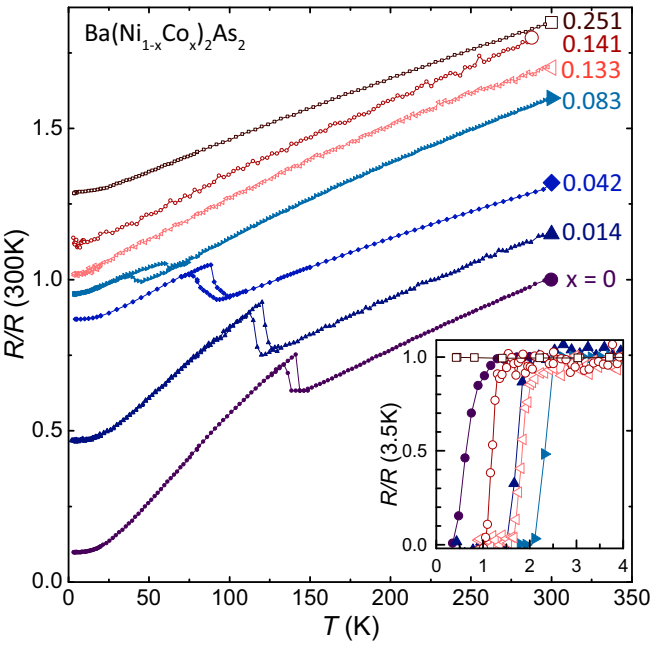

FIG. 3. Transport measurements in $Ba(Ni_{1-x}Co_x)_2As_2$ single crystals grown from Pb flux. Main figure displays resistance normalized to room-temperature value, and vertically offset for clarity. Data show clear suppression of anomalies associated with the structural transition, which vanishes by $x = 0.133$. Inset displays low-temperature resistance normalized to 3.5 K value. Samples display clear enhancement of T_c when approaching structural phase boundary. Data plotted in blue ($x \leqslant 0.083$) feature a low-temperature resistance anomaly consistent with the triclinic structural distortion. Curves plotted in red remain tetragonal down to the lowest measured temperature.

III. RESULTS

The electrical resistivity of NiAs-grown $BaNi_2As_2$ is presented in Fig. 2, showing a pronounced hysteresis in the data collected on warming and cooling due to the strongly first-order tetragonal to triclinic structural transition. This hysteresis is also observed in the magnetic susceptibility [see inset (a) to Fig. 2] and heat capacity [see inset (b) to Fig. 2]. Figure 3 displays the evolution of the hysteretic region in $Ba(Ni_{1-x}Co_x)_2As_2$ as measured by resistivity on heating and cooling. The hysteresis, and by extension the structural distortion, is observed throughout the range of the triclinic phase and is quickly suppressed with increasing x. Extrapolating this data, we determine that the structural transition vanishes entirely at concentration $x_c = 0.11$. This observation is consistent with the evolution of the heat capacity anomaly shown in Fig. 4, which also is absent by $x = 0.133$. The low-temperature heat capacity displayed in the inset to Fig. 4 shows no dramatic changes in Debye temperature and a monotonically increasing Sommerfield coefficient for the reported Co concentrations. The Sommerfield coefficient is enhanced from 10 mJ/mol K^2 to nearly 16 mJ/mol K^2 between $x = 0.013$ and $x = 0.083$. The extracted Debye temperatures are $\Theta_D = 236$, 218 K, and 225 K for $x = 0.014$, 0.083, and 0.133, respectively. Pure $BaNi_2As_2$ was observed to have a Debye temperature of 250 K, consistent with previous work [13].

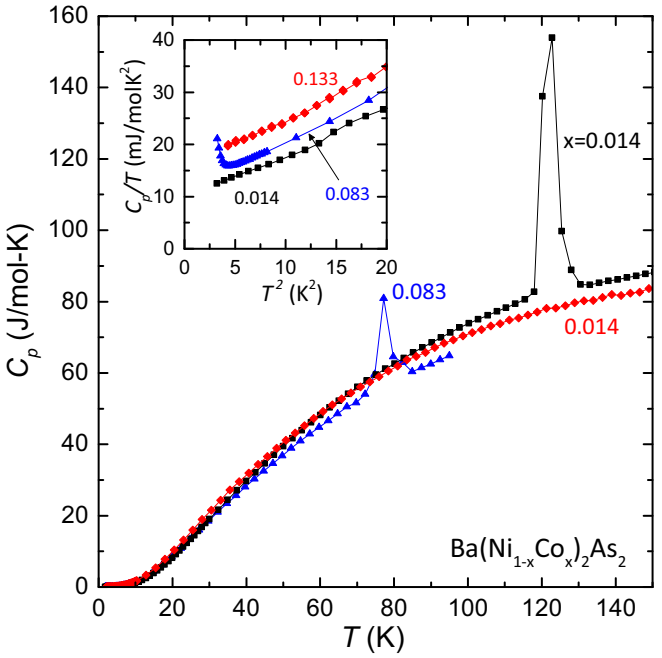

FIG. 4. Heat capacity measurements collected on warming in $Ba(Ni_{1-x}Co_x)_2As_2$ crystals grown from Pb flux. Anomalies in the main figure are indicative of structural transition. Inset displays low-temperature C_p/T data plotted versus temperature squared.

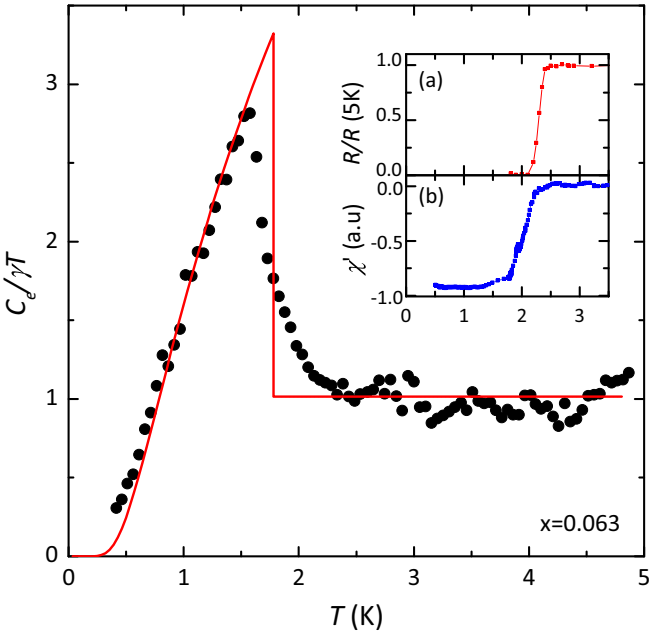

FIG. 5. Measurements of superconducting transition in sample with near optimal substitution $x = 0.063$ grown from Pb flux. Electronic heat capacity (C_e) was determined by subtracting the phonon contribution (βT^3) from the total heat capacity (main figure). Red curve is the α-model predictions for a BCS superconductor [30] ($\alpha = 1.764$) scaled by a constant multiple to match the data. Inset displays superconducting transition measured via four-terminal resistance (a) and the real part of ac susceptibility measured using a homemade coil (b).

Despite large changes in low-temperature structure, superconductivity surprisingly evolves continuously in the $Ba(Ni_{1-x}Co_x)_2As_2$ series (see Fig. 3, inset), with a fast enhancement in T_c upon cobalt substitution, rising from $T_c = 0.7$ K at $x = 0$ to 1.7 K with just 1.4% cobalt substitution for nickel. T_c continues to increase with x in the triclinic phase, eventually exhibiting a maximum of 2.3 K at $x = 0.083$ and then gradually decreasing until entirely absent by $x = 0.251$. Although small crystal sizes complicate dc-magnetization measurements in these samples, the observation of enhanced superconductivity rather than its rapid suppression for small x suggests that Co behaves as a nonmagnetic substituent in the $Ba(Ni_{1-x}Co_x)_2As_2$ series.

Figure 5 presents heat capacity (main), transport (a), and ac magnetization (b) measurements of the superconducting transition in the same single-crystal sample (crystal dimensions of 0.67 mm × 0.83 mm × 0.067 mm) with $x = 0.063$. Balancing the entropy in the observed heat capacity jump yields a T_c of 1.8 K for this sample. The red curve in Fig. 5 is the α model prediction of heat capacity for a single band BCS superconductor. This curve has been scaled by a constant value of 1.35 to match the observed heat capacity jump. This model describes data well near T_c, and deviations at low temperatures may be due to nuclear Schottky contributions as observed in the pure compound [16]. The modeled heat capacity jump $\Delta C_e/\gamma T$ is ∼2.2, well above the BCS limit of 1.43, indicating strongly coupled superconductivity at this Co concentration. This value is consistent with previous reports of enhanced normalized heat capacity jumps of approximately 1.9 in both $Ba(Ni_{1-x}Cu_x)_2As_2$ and $BaNi_2(As_{1-x}P_x)_2$ [21,22] and greatly exceeds the near-BCS value observed in pure $BaNi_2As_2$ [16]. While previous work on Cu- and P-substituted $BaNi_2As_2$ suggested that the enhancement in the tetragonal phase was consistent with a phonon softening picture, this is not the case here, as the enhancement occurs in the triclinic phase and the Debye frequency exhibits little change through the entire Co substitution range as noted above.

Both superconductivity and the structural transition in optimally substituted $x = 0.083$ samples were observed to be of bulk origin, as each manifested itself in anomalies in measured heat capacity (see Fig. 4, main and inset). Figure 6 shows the evolution of upper critical field in these optimally substituted samples, which exhibit an approximately threefold enhancement compared to the pure compound. As reported in $BaNi_2As_2$, superconductivity in optimally substituted $Ba(Ni_{1-x}Co_x)_2As_2$ is more robust when the field is applied parallel to the crystal plane. At higher fields, resistance curves taken in this orientation begin to broaden, while data taken with the field along the c axis remain sharp over all measurements. H_{c2} anisotropy, Γ, remains virtually constant at all temperatures, with $\Gamma = 1.50$ slightly below the value 2.1 reported for the pure compound [12].

IV. DISCUSSION

Previous reports of chemical substitution in $BaNi_2As_2$ feature nearly identical evolutions of superconductivity. However, this trend is broken through Co substitution, which causes a strong enhancement of T_c *within* the triclinic phase and a smooth evolution through the triclinic-tetragonal $T = 0$

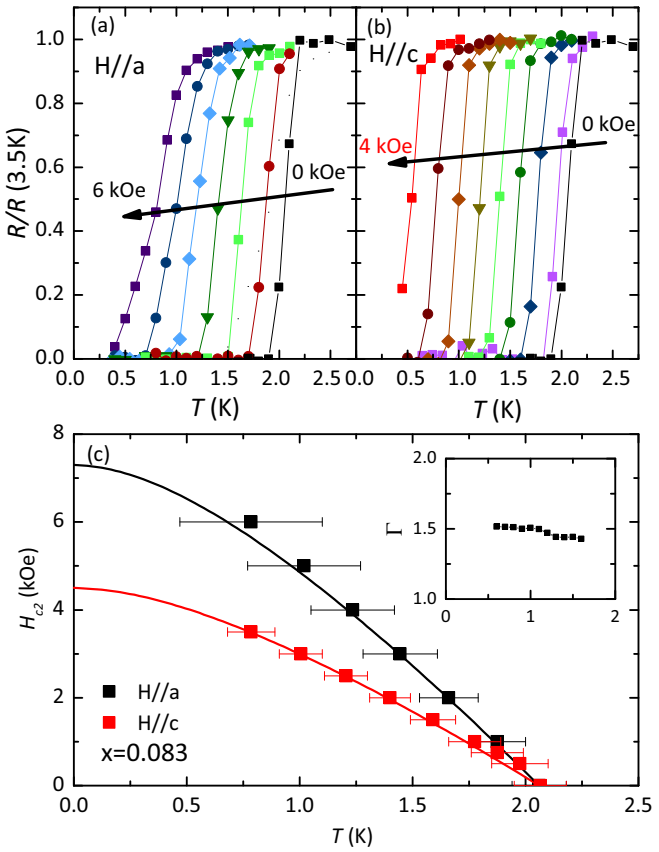

FIG. 6. H_{c2} data collected on an optimally substituted sample of $x = 0.083$ grown from Pb flux. Isomagnetic resistance data collected with field parallel to crystal a axis (a) and parallel to crystal c axis (b). Data collected parallel to the c axis were taken in 0.5 kOe increments (0, 0.5, 1, 1.5, 2, 2.5, 3, 3.5, and 4 kOe), while measurements with $H \parallel a$ were taken in 1 kOe increments (0, 1, 2, 3, 4, 5, and 6 kOe). (c) H_{c2} vs T_c phase diagram in parallel and perpendicular configuration. Data points were taken at the midpoint of the resistive transition, and error bars represent the range wherein resistance is between 90% and 10% of the normal state value. Curves are generated for a dirty BCS superconductor using the model developed by Werthamer *et al.* [31]. Inset shows upper critical field anisotropy, Γ, determined using the midpoint criteria.

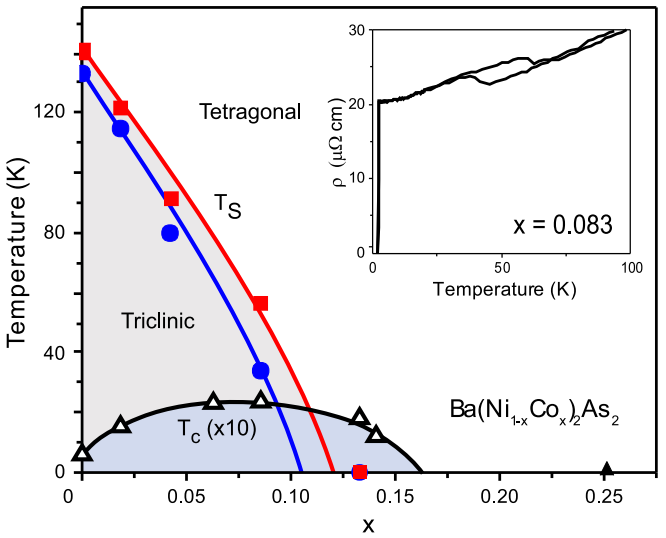

FIG. 7. Phase diagram for the $Ba(Ni_{1-x}Co_x)_2As_2$ system gathered from transport data in single crystals grown from Pb flux. Structural and superconducting critical temperatures were both determined by the midpoint of each resistive transition. Red (blue) symbols denote the tetragonal-triclinic transition on warming (cooling) as gathered from transport measurements. Superconducting T_c is scaled by a factor of 10 to improve clarity. Inset displays transport data for optimally substituted, $x = 0.083$, samples featuring both clear enhancement in T_c and structural transition anomaly.

boundary, manifesting in a superconducting dome-shaped phase diagram (Fig. 7).

Previous reports suggest the $BaFe_2As_2$, $BaCo_2As_2$, and $BaNi_2As_2$ electronic structures differ through only a rigid shift in the chemical potential [17,32]. Calculations in the $Ba(Ni_{1-x}Co_x)_2As_2$ series, however, show a monotonic enhancement in electronic density of states (DOS) at E_F with increasing Co (Fig. 8) due to a Co d-orbital component that smoothly adds to the total DOS rather than a rigid band shift. The calculated DOS(E_F) is 1.81, 2.02, and 2.09 states/eV for $x = 0$, 0.125, and 0.25, respectively. Although the DOS behavior in triclinic $BaNi_2As_2$ cannot be inferred from these calculations, calculations in $x = 0.125$ and 0.25 reflect the true ground-state DOS, the enhancement of which could be expected to provide an environment more hospitable to superconductivity. The observed suppression of T_c with high Co concentration is inconsistent with these results, ruling out changes in DOS as the predominant factor responsible for enhanced T_c. We also observe no dramatic changes to Fermi surface topology that account for the rapid suppression of superconductivity in oversubstituted $Ba(Ni_{1-x}Co_x)_2As_2$. While the enhanced

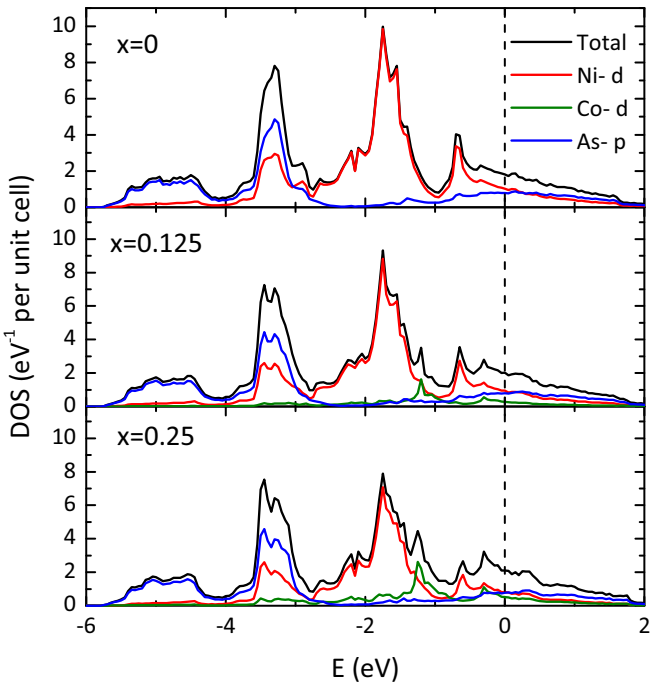

FIG. 8. The evolution of the electronic density of states in $Ba(Ni_{1-x}Co_x)_2As_2$. All calculations were taken for samples in the tetragonal phase using experimentally determined lattice parameters. Data displayed for $x = 0$ (top), 0.125 (center), and 0.25 (bottom).

Wilson ratio observed in the Co-based end-member $BaCo_2As_2$ [32] suggests that increasing Co concentration may ultimately invoke ferromagnetic correlations, the concentrations where T_c is suppressed in $Ba(Ni_{1-x}Co_x)_2As_2$ series are far from $x = 1$ such that it is unlikely that the rapid suppression of T_c in the tetragonal phase is a result of proximity to ferromagnetism, and warrants further investigation.

$Ba(Ni_{1-x}Cu_x)_2As_2$ and $BaNi_2(As_{1-x}P_x)_2$ series also exhibit phonon softening in high-T_c samples, indicated by strong superconducting coupling and a dramatically reduced Debye temperature. While strong superconducting coupling is also observed in the $Ba(Ni_{1-x}Co_x)_2As_2$ series, the Debye temperature remains virtually constant over the range of x studied here. Given the strongly first-order nature of the structural transition, phonon softening within the triclinic phase is unexpected, although would not be unprecedented [33]. While the effect of phonon softening on pairing near such a strongly discontinuous structural boundary cannot be ignored, the distinct behavior found in the $Ba(Ni_{1-x}Co_x)_2As_2$ series suggests another mechanism is responsible for the strengthening of superconductivity, which appears to be centered around x_c. The recent observations of CDW order in $BaNi_2As_2$ [24] are a provocative suggestion that the previously mundane view of both superconductivity and the structural distortion in $BaNi_2As_2$ should be revisited, and that fluctuation-driven superconductivity is a real possibility [15]. Further, uncovering a new mechanism for superconducting enhancement opens an interesting avenue to potentially extend superconductivity to even higher critical temperatures in this and related systems.

ACKNOWLEDGMENTS

Research at the University of Maryland was supported by the AFOSR under Grant No. FA9550-14-10332 and the Gordon and Betty Moore Foundation under Grant No. GBMF4419. We also acknowledge support from the Center for Nanophysics and Advanced Materials as well as the Maryland Nanocenter and its FabLab.

[1] Y. Kamihara, T. Watanabe, M. Hirano, and H. Hosono, J. Am. Chem. Soc. **130**, 3296 (2008).
[2] J. Paglione and R. Greene, Nat. Phys. **6**, 645 (2010).
[3] D. C. Johnston, Adv. Phys. **59**, 803 (2010).
[4] M. D. Lumsden and A. D. Christianson, J. Phys.: Condens. Matter **22**, 203203 (2010).
[5] M. Rotter, M. Tegel, D. Johrendt, I. Schellenberg, W. Hermes, and R. Pöttgen, Phys. Rev. B **78**, 020503 (2008).
[6] R. M. Fernandes, A. V. Chubukov, and J. Schmalian, Nat. Phys. **10**, 97 (2014).
[7] P. C. Canfield and S. L. Bud'ko, Annu. Rev. Condens. Matter Phys. **1**, 27 (2010).
[8] G. R. Stewart, Rev. Mod. Phys. **83**, 1589 (2011).
[9] F. Hardy, P. Burger, T. Wolf, R. A. Fisher, P. Schweiss, P. Adelmann, R. Heid, R. Fromknecht, R. Eder, D. Ernst, H. v. Lhneysen, and C. Meingast, Europhys. Lett. **91**, 47008 (2010).
[10] M. Abdel-Hafiez, Y. Zhang, Z. He, J. Zhao, C. Bergmann, C. Krellner, C.-G. Duan, X. Lu, H. Luo, P. Dai, and X.-J. Chen, Phys. Rev. B **91**, 024510 (2015).
[11] K. Hashimoto, M. Yamashita, S. Kasahara, Y. Senshu, N. Nakata, S. Tonegawa, K. Ikada, A. Serafin, A. Carrington, T. Terashima, H. Ikeda, T. Shibauchi, and Y. Matsuda, Phys. Rev. B **81**, 220501 (2010).
[12] F. Ronning, N. Kurita, E. D. Bauer, B. L. Scott, T. Park, T. Klimczuk, R. Movshovich, and J. D. Thompson, J. Phys.: Condens. Matter **20**, 342203 (2008).
[13] A. S. Sefat, M. A. McGuire, R. Jin, B. C. Sales, D. Mandrus, F. Ronning, E. D. Bauer, and Y. Mozharivskyj, Phys. Rev. B **79**, 094508 (2009).
[14] K. Kothapalli, F. Ronning, E. D. Bauer, A. J. Schultz, and H. Nakotte, J. Phys.: Conf. Ser. **251**, 012010 (2010).
[15] Y. Yamakawa, S. Onari, and H. Kontani, J. Phys. Soc. Jpn. **82**, 094704 (2013).
[16] N. Kurita, F. Ronning, Y. Tokiwa, E. D. Bauer, A. Subedi, D. J. Singh, J. D. Thompson, and R. Movshovich, Phys. Rev. Lett. **102**, 147004 (2009).
[17] A. Subedi and D. J. Singh, Phys. Rev. B **78**, 132511 (2008).
[18] I. I. Mazin, D. J. Singh, M. D. Johannes, and M. H. Du, Phys. Rev. Lett. **101**, 057003 (2008).
[19] N. Ni, A. Thaler, J. Q. Yan, A. Kracher, E. Colombier, S. L. Bud'ko, P. C. Canfield, and S. T. Hannahs, Phys. Rev. B **82**, 024519 (2010).
[20] F. Ronning, E. Bauer, T. Park, N. Kurita, T. Klimczuk, R. Movshovich, A. Sefat, D. Mandrus, and J. Thompson, Physica C (Amsterdam) **469**, 396 (2009).
[21] K. Kudo, M. Takasuga, and M. Nohara, arXiv:1704.04854.
[22] K. Kudo, M. Takasuga, Y. Okamoto, Z. Hiroi, and M. Nohara, Phys. Rev. Lett. **109**, 097002 (2012).
[23] T. Mine, H. Yanagi, T. Kamiya, Y. Kamihara, M. Hirano, and H. Hosono, Solid State Commun. **147**, 111 (2008).
[24] S. Lee, G. de la Pena, S. Sun, Y. Fang, M. Mitrano, H. Jang, J. Lee, C. Eckberg, D. Campbell, J. Collini, J. Paglione, F. de Groot, and P. Abbamonte, arXiv:1801.04874.
[25] K. Schwarz, P. Blaha, and G. Madsen, Comput. Phys. Commun. **147**, 71 (2002).
[26] W. Ku, T. Berlijn, and C.-C. Lee, Phys. Rev. Lett. **104**, 216401 (2010).
[27] S. Yonezawa, T. Higuchi, Y. Sugimoto, C. Sow, and Y. Maeno, Rev. Sci. Instrum. **86**, 093903 (2015).
[28] See https://education.qdusa.com/edu_files/EM_QD_200_01.pdf.
[29] See Heat Capacity manual, Quantum Design Physical Property Measurement System .
[30] D. C. Johnston, Supercond. Sci. Technol. **26**, 115011 (2013).
[31] N. R. Werthamer, E. Helfand, and P. C. Hohenberg, Phys. Rev. **147**, 295 (1966).
[32] A. S. Sefat, D. J. Singh, R. Jin, M. A. McGuire, B. C. Sales, and D. Mandrus, Phys. Rev. B **79**, 024512 (2009).
[33] D. Hirai, F. von Rohr, and R. J. Cava, Phys. Rev. B **86**, 100505 (2012).